Velocity Dependence of Dark Matter Electron Scattering

Tess W.P. Jacobson
Department of Physics, Princeton University

Advisor: Mariangela Lisanti

Abstract

The detection of ionization signals from dark matter-electron scattering is a promising channel for direct detection experiments, which are currently confined to high energy thresholds and dark matter (DM) masses above the GeV scale. In the following paper, I will review the calculation of the scattering rate for both the DM-nucleus and DM-electron scattering cases, and study the implications of experiments using the empirical distribution for DM velocity from Herzog-Arbeitman *et al.* (2017) rather than the most commonly used Standard Halo Model velocity distribution. I provide a general introduction to dark matter and a review of different formulations of the DM velocity distribution, followed by derivations of the formula for the differential scattering rate of a dark matter particle off of a nuclear target as well as a derivation of the differential rate for DM-electron scattering events in an atomic target. These calculations are repeated in Section 3 using both the SHM velocity distribution and the empirical distribution. The empirical distribution creates larger scattering rates than the SHM at higher electron recoil energies, and the difference between the rates from the empirical distribution and the SHM becomes more pronounced as the dark matter mass is reduced.

This paper represents my own work in accordance with University regulations.

/s/ Tess Jacobson

1 Introduction to Dark Matter

Dark matter makes up nearly 85% of the Universe's matter density [1]. Yet it does not absorb or reflect light, and so both the strongest evidence for the existence of dark matter and the basic assumptions that can be made about the nature of DM are drawn from observing the gravitational interactions between DM and visible matter in the universe.

1.1 Rotation Curves

We will consider the orbital velocities of stars in order to trace the gravitational effects of DM. Stars in a disk galaxy are essentially collisionless, so their motion is largely dictated by gravitational interactions. A *rotation curve* of a star plots the rotational velocity of that star versus its distance from the center of the Galactic disk. The discrepancy between observed and theoretical rotation curves described below provided the first strong evidence for the existence of dark matter.

The orbital velocity of a star can be found by a basic Newtonian calculation, setting centripetal force equal to gravitational force:

$$\frac{mv^2}{r} = \frac{GMm}{r^2},$$

where m is the mass of the star, v is the star's circular velocity, M is the enclosed mass, and r is the radial distance from the center of the Galactic disk. The mass of the star cancels out, and this reduces to

$$v = \sqrt{\frac{GM}{r}}.$$

For a Galactic disk of radius R_{disk}, when r $> R_{disk}$ and assuming all the enclosed mass is within the disk, the orbital velocity should go as $v \propto r^{-1/2}$. However, observations of stars in the Galactic disk actually show their rotation curves flattening out at distances beyond the disk, so that v goes like a constant and therefore the enclosed mass must be proportional to distance r. This implies that there is additional matter in the system aside from the visible matter in the disk. These results, and thus the first strong evidence for the existence of non-baryonic matter, were revealed in a seminal 1980 paper by Rubin *et al.* [2] (Fig. 1 shows the flattening rotation curves in this paper). Assuming this matter is distributed in a spherically symmetric halo about the center of the disk, we can infer that the dark matter density distribution must go like

$$\rho(r) \propto \frac{M(r)}{r^3} \sim \frac{1}{r^2}. \tag{1}$$

The local dark matter density in the Milky Way is taken to be $\rho_0 \sim 0.3\ GeV/cm^3$ [3].

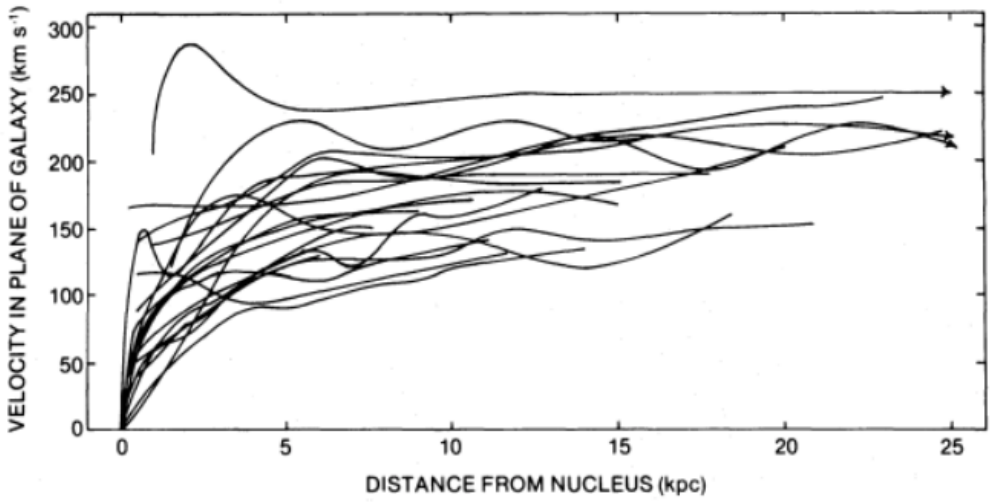

Figure 1: 21 Sc flattening rotation curves from Rubin *et al.* [2].

1.2 Velocity Distribution

A given DM density distribution has an associated velocity distribution, which is an important function for the purposes of studying the physics behind dark matter detection experiments.

1.2.1 Standard Halo Model

The dark matter velocity distribution can be derived explicitly using the density distribution of $\rho(r) \propto \frac{1}{r^2}$, because the density and velocity distributions of an isotropic DM halo are related through the gravitational potential. The velocity distribution consistent with an inverse-square density distribution is a Maxwellian. I will follow the derivation of this velocity distribution given in [3]. First, the derivation requires the Boltzmann equation, which gives the time evolution of $f(\mathbf{x}, \mathbf{v})$, the phase-space density of a dark-matter particle in the isotropic halo. The Boltzmann equation states:

$$\mathbf{L}[f(\mathbf{x}, \mathbf{v})] = \mathbf{C}[f(\mathbf{x}, \mathbf{v})], \tag{2}$$

where $\mathbf{L}$ is the Liouville operator, and $\mathbf{C}$ is the collision operator. The non-relativistic form of the Liouville operator is:

$$\mathbf{L}[f(\boldsymbol{x}, \boldsymbol{v})] = \frac{\partial f}{\partial t} + \dot{\mathbf{x}}\frac{\partial f}{\partial \mathbf{x}} + \dot{\mathbf{v}}\frac{\partial f}{\partial \mathbf{v}},$$

and since we are dealing with a non-relativistic and collisionless DM halo, the right-hand side of the Boltzmann equation is zero, and we have:

$$\frac{\partial f}{\partial t} + \dot{\mathbf{x}}\frac{\partial f}{\partial \mathbf{x}} + \dot{\mathbf{v}}\frac{\partial f}{\partial \mathbf{v}} = 0. \tag{3}$$

Now, Jeans's theorem states that any steady-state solution to the collisionless Boltzmann equation (3) must only depend on the phase-space coordinates through the integrals of motion, which are all functions of only the phase-space coordinates that remain constant with time, including the Hamiltonian (see Chapter 4 of [4] for a more in-depth review of the collisionless Boltzmann equation and Jeans's Theorem). In this case, Jeans's Theorem implies that the distribution $f(\mathbf{x}, \mathbf{v})$ must be a function of only the energy $\mathcal{E}$, so:

$$f(\mathbf{x}, \mathbf{v}) = f(\mathcal{E}), \text{ where } \mathcal{E} = \Psi - \frac{v^2}{2}$$

and where Ψ is the gravitational potential. If we guess that the energy dependence of the velocity distribution is $f(\mathcal{E}) \propto e^{\mathcal{E}}$, or more precisely, $f(\mathcal{E}) = e^{\mathcal{E}/\sigma^2} \propto e^{-v^2/\sigma^2}$ where σ is the RMS velocity dispersion, we can calculate the associated density distribution:

$$\rho \propto \int_0^\infty dv\ v^2 f(v) = \int_0^\infty dv\ v^2 \exp\left(\frac{\Psi - v^2/2}{\sigma^2}\right) \propto e^{\Psi/\sigma^2},$$

and therefore, $\Psi \propto \ln \rho$. Now, using the spherically symmetric form of Poisson's equation, we can solve for the density distribution in terms of r:

$$\begin{aligned} \frac{1}{r^2}\frac{\mathrm{d}}{\mathrm{d}r}(r^2\frac{\mathrm{d}\Psi}{\mathrm{d}r}) &= -4\pi G\rho \\ \implies \rho(r) &= \frac{\sigma^2}{2\pi G r^2} \propto \frac{1}{r^2}. \end{aligned}$$

This is an inverse-square density distribution, as in equation (1). Thus, the velocity distribution for an isotropic, steady-state DM halo consistent with the inverse-square density distribution is described by a Maxwell-Boltzmann distribution:

$$f(v) \propto e^{-v^2/\sigma^2}. \tag{4}$$

The form of the DM velocity distribution used most commonly in the literature is called the Standard Halo Model, and takes the form:

$$f(\boldsymbol{v}) = \begin{cases} \frac{1}{N_{esc}}(\frac{3}{2\pi\sigma^2})^{3/2} e^{3\boldsymbol{v}^2/2\sigma^2} & \text{if } |\boldsymbol{v}| < v_{esc}, \\ 0 & \text{otherwise.} \end{cases} \tag{5}$$

where $N_{esc} = \mathrm{erf}(z) - 2\pi^{-1/2} z e^{-z^2}$ with z $\equiv v_{esc}/v_0$, $v_{esc} \approx 544$ km/s is the Galactic escape velocity [5], σ is the RMS velocity dispersion, and $v_0 = \sqrt{2/3}\sigma_v \approx 235$ km/s is the most probable speed [3].

While the Maxwell-Boltzmann velocity distribution is consistent with a density distribution of $\rho(r) \propto \frac{1}{r^2}$, the distribution for an isothermal sphere of particles, numerical simulations of Milky-Way-like dark matter halos have resulted in several widely-used profiles that differ from the isothermal approximation. These numerical simulations are called N-body simulations, as they account for the many-bodied merging of galaxies and

gravitational interactions between DM halos as they merge. In the Lambda cold dark matter (ΛCDM) framework, the Milky Way's DM halo forms from the historical hierarchical merging of subhalos, and many of these N-body simulations trace the formation of Milky-Way-like halos and their merging events [6]. Some of the highest-resolution simulations that model dark matter halos on the scale of the Milky Way are `Via Lactea II` [7], `GHALO` [8], and `Aquarius` [9]. These simulations include only dark matter, as opposed to full hydrodynamic simulations, which include gas and stellar distributions. See [10] for expected dark matter velocity distributions produced using the `Via Lactea II` and `GHALO` simulations. The first realistic simulation of the distributions of dark matter, gas, and stars in a Milky-Way-like spiral galaxy was `Eris`, in 2011 [11]. The distributions from DM-only simulations were found to have more high velocity particles than the Standard Halo Model [12], while simulations that account for baryons are generally more consistent with the SHM [13]. In addition, the FIRE (Feedback In Realistic Environments) Project produces galaxy formation simulations such as the `Latte Project: The Milky Way on FIRE` [6], which produced a simulation of low-mass "dwarf galaxies" (where $M_{star} \leq 10^9 M_\odot$).

Several theoretical dark matter density profiles have resulted from numerical simulations of our Galaxy. The Navarro-Frenk-White (NFW) profile was proposed in 1995 using N-body simulations of dark matter halos and models the density distribution as such [14].

$$\rho_{NFW}(r) = \frac{\rho_0}{\frac{r}{r_s}(1+\frac{r}{r_s})^2},$$

where r_s is a scale radius. Another commonly used profile, the Einasto profile, models the dark matter density distribution as [15, 16]:

$$\rho_{Ein}(r) = \rho_0 \exp\left[-\frac{2}{\gamma}((\frac{r}{r_s})^\gamma - 1)\right],$$

where $\gamma = 0.17$ [15]. This is all to say that the isothermal density distribution and the Standard Halo Model do not model dark matter halos exactly, and the widely-used Standard Halo Model velocity distribution is not completely consistent with the density profiles provided by numerical simulations.

1.2.2 RAVE-TGAS Empirical Distribution

Alternative DM velocity distributions can be produced empirically using tracers as well. For example, in a 2017 letter by Herzog-Arbeitman *et al.* [13], it was shown using data from the `Eris` simulation that metal-poor halo stars in the Solar neighborhood served as reliable tracers for the virialized dark matter velocity distribution, because old stars in the halo share a merger history with the Milky Way DM halo in the ΛCDM paradigm. Metal-poor stars are chosen because a star's metallicity indicates its origins, and it has been shown that the inner stellar halo ($\sim$20 kpc) of the Milky Way is metal-poor, with iron abundance of [Fe/H] ~ -1.5 [17], where the stellar abundance [X/Y] of element X

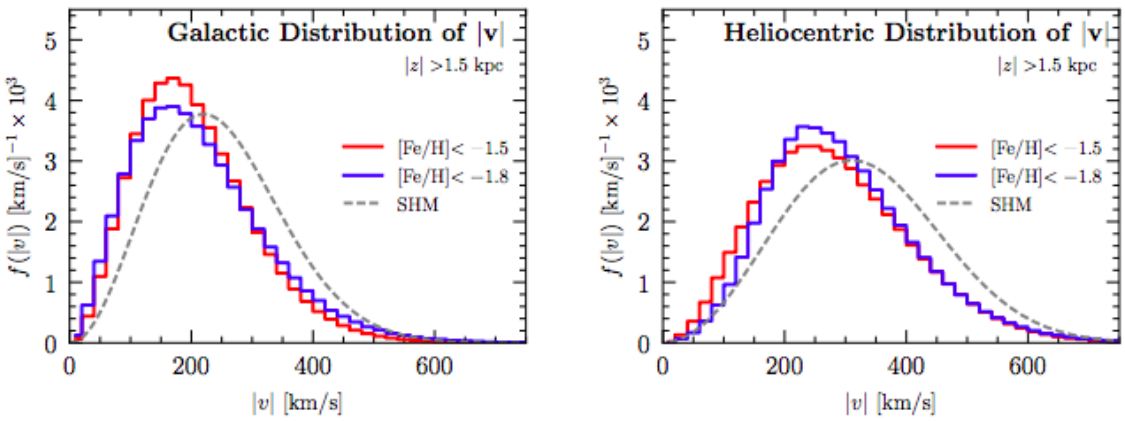

Figure 2: Empirical velocity distributions for metal-poor stars in the RAVE-TGAS halo. Distributions for iron abundancies [Fe/H] < -1.5 (red) and [Fe/H] < -1.8 (blue) are shown for the Galactic frame (left) and the heliocentric frame (right), and the Standard Halo Model distribution is shown in dotted black. Figure from [18].

with respect to element Y is defined as:

$$[\mathrm{X/Y}] = \log_{10}(N_X/N_Y)_{\mathrm{star}} - \log_{10}(N_X/N_Y)_{\odot},$$

where the N_i's are the number of atoms of element i per unit volume [13].

In a later 2017 paper [18], Herzog-Arbeitman *et al.* used the kinematic data of stars with iron abundancies [Fe/H] < -1.5 and [Fe/H] < -1.8 to produce empirical dark matter velocity distributions. Data from the first *Gaia* spacecraft data release was used [19], specifically, the *Tycho-Gaia* astronomical solution (TGAS), which provides information on the motion of the subset of stars which overlap in both the `HIPPARCOS` and *Tycho-2* catalogs. This data was combined with data from the RAdial Velocity Experiment (RAVE) [20] to create the RAVE-TGAS catalog of six-dimensional phase space of the local stellar halo, and new empirical DM velocity distributions were produced. Fig. 2 shows these empirical distributions as compared to the Standard Halo Model. The empirical distributions both peak around ~ 170 km/s, a lower speed than the SHM, and they also predict fewer high-velocity dark matter particles for v $\gtrsim 200$ km/s.

2 Direct Detection and Scattering Rates

Dark matter direct detection experiments involve the placement of a low-background underground sensor waiting for dark matter to scatter off a particle in the detector, so that the recoil of the baryonic particle can be detected and inferences about the nature of the dark matter particle can be made. To get a sense of the interactions of dark matter particles on Earth, billions of dark matter particles are thought to pass through an average human body every second, while only approximately 10 will scatter off of a nucleus in the

human body throughout the course of one year [21]. The rest of this section will review the physics of direct detection experiments, for both the cases of a nuclear target and an electron target.

2.1 Nuclear Case

2.1.1 Dark Matter-Nucleus Kinematics

Imagine a dark matter particle with mass m_χ colliding with a stationary nucleus of mass m_N, resulting in momentum transfer q. The recoil energy of the nucleus, E_R, is then

$$E_R = \frac{|q|^2}{2m_N}. \tag{6}$$

In the elastic scattering regime, we can find v_{min}, the minimum velocity of the incoming dark matter required for the nucleus to recoil with energy E_R, by rewriting the momentum transfer q in equation (6) and examining the kinematics of an elastic dark matter-nucleus collision more closely:

$$\boldsymbol{q} = \boldsymbol{p}_{\chi,f} - \boldsymbol{p}_{\chi,i}, \tag{7}$$

In the center-of-mass frame for this collision, the dark matter momentum ($\boldsymbol{p}_\chi$) and the nucleus momentum ($\boldsymbol{p}_N$) are equal and opposite. The initial dark matter momentum in the center-of-mass frame is:

$$\boldsymbol{p}_{\chi,i} = -\boldsymbol{p}_{N,i} = \mu \boldsymbol{v}, \tag{8}$$

where $\mu = \frac{m_\chi m_N}{m_\chi + m_N}$ is the reduced mass of the dark matter-nucleus system and $\boldsymbol{v}$ is the velocity of the incoming dark matter. Using (6) and (7), the final dark matter momentum in this frame is then:

$$\boldsymbol{p}_{\chi,f} = -\boldsymbol{p}_{N,f} = \boldsymbol{q} + \mu \boldsymbol{v}. \tag{9}$$

For an elastic collision in this frame, $|\boldsymbol{p}_{\chi,i}| = |\boldsymbol{p}_{\chi,f}| = p_\chi^2$, and so we can write the momentum transfer squared as:

$$\begin{aligned} |q|^2 &= 2(|\boldsymbol{p}_{\chi,i}|^2 - \boldsymbol{p}_{\chi,i} \cdot \boldsymbol{p}_{\chi,f}) \\ &= 2{p_\chi}^2(1 - \cos\theta) \\ &= 2\mu^2 v^2 (1 - \cos\theta), \end{aligned} \tag{10}$$

where θ is the scattering angle of the nucleus in the lab frame. Using equation (10) and maximizing with respect to θ, the recoil energy E_R is thus bound:

$$E_R = \frac{\mu^2 v^2}{m_N}(1 - \cos\theta) \leq \frac{2\mu^2 v^2}{m_N}, \tag{11}$$

and therefore the minimum dark matter velocity required for a nuclear scattering with recoil energy E_R can be expressed as:

$$v_{min} = \sqrt{\frac{m_N E_R}{2\mu^2}}. \tag{12}$$

2.1.2 Nuclear Scattering Rate Calculation

The basic scattering rate of particles in a dark matter-nucleus collision is given by

$$R = n_\chi \sigma v,$$

where n_χ is the number density of the incoming dark matter particles, σ is the scattering cross section of the nucleus, and v is the velocity of the incoming dark matter. The quantity of interest for direct detection experiments, however, is the differential scattering rate $\frac{dR}{dE_R}$:

$$\frac{dR}{dE_R} = \frac{n_\chi}{m_N} \left\langle v \frac{d\sigma}{dE_R} \right\rangle,$$

where again, $n_\chi = \rho_\chi / m_\chi$ is the dark matter number density (and ρ_χ is the same as the local dark matter density $\rho_0 \approx 0.3 GeV/cm^3$ as defined in Section 1.1), σ is the scattering cross section of the nucleus, and v is the velocity of the incoming dark matter, and the bracketed term is averaged over the velocities of the incoming dark matter. Writing this average as an integral, the full form of the scattering rate is

$$\frac{dR}{dE_R} = \frac{\rho_\chi}{m_N m_\chi} \int_{v_{min}}^{v_{max}} v \tilde{f}(\mathbf{v}, t) \frac{d\sigma}{dE_R} d^3 v, \tag{13}$$

where v_{min} is the minimum velocity required for the nucleus to scatter with recoil energy E_R (calculated above), v_{max} is the escape velocity $v_{esc} \approx 544$ km/s from Section 1.2.1, and $\tilde{f}(\boldsymbol{v}, t)$ is the dark matter velocity distribution in the lab frame. The SHM equation for $f(\boldsymbol{v})$ in Section 1.2.1 is in the Galactic frame, and so the lab frame distribution $\tilde{f}(\mathbf{v}, t)$ can be approximated as applying a Galilean boost to the Galactic frame equation:

$$\tilde{f}(\mathbf{v}, t) = f(\mathbf{v} + \mathbf{v}_{obs}(t)), \text{where } \mathbf{v}_{obs}(t) = \mathbf{v}_\odot + \mathbf{V}_\oplus(t).$$

$\mathbf{v}_{obs}(t)$ is the velocity of the detector in the Galactic frame, $\mathbf{v}_\odot$ is the velocity of the Sun relative to the dark matter, and $\mathbf{V}_\oplus(t)$ is the velocity of the Earth about the Sun, with a time dependence from the annular modulation of the Earth about the Sun and Earth's rotation about its axis. For the purposes of this paper, we will not worry about the time dependence of $\mathbf{v}_{obs}(t)$ and take the value given in the appendix of [22] for June, when the Earth's velocity relative to the DM halo is at its peak and $\mathrm{v}_{obs} \approx 27$ km/s. For a more detailed review of the time dependence of direct detection experiments, see [23].

Finally, the rate calculation requires $\frac{d\sigma}{dE_R}$, the differential scattering cross section. This cross section depends on whether the interaction is spin-independent or spin-dependent. For the purposes of this paper, I will use the spin-independent formula from [3]:

$$\frac{d\sigma}{dE_R} = \frac{2 m_N}{4 \mu_p^2 v^2} F^2(q) \sigma_{SI}, \tag{14}$$

where σ_{SI} is the DM-*nucleus* cross section. Since direct detection experiements use several different target nuclei, we can factor out the dependence on the target nucleus by using

the DM-*nucleon* cross section and reduced mass, σ_p and μ_p, respectively, and A, the mass number of the target:

$$\sigma_{SI} = \frac{\mu^2}{\mu_p^2} A^2 \sigma_p, \text{ so that } \frac{d\sigma}{dE_R} = \frac{m_N}{2\mu_p^2 v^2} F^2(q) A^2 \sigma_p. \tag{15}$$

$F(q)$ is the nuclear form factor, which accounts for the the fact that at large enough momentum transfer q (when the wavelength h/q becomes comparable or small in relation to the size of the nucleus), the effective cross-section decreases as q increases. $F(q)$ is approximated by the Fourier transform of the mass distribution of the nucleus, and is commonly described by the Helm form factor [24]:

$$F(q) = 3e^{q^2 s^2/2} \frac{\sin(qr_n) - qr_n \cos(qr_n)}{(qr_n)^3}, \tag{16}$$

where r_n is the nuclear radius, given by $r_n^2 = c^2 + \frac{7}{3}\pi a^2 - 5s^2$, $a \approx 0.52$ fm, $s \approx 0.9$ fm, and $c \approx 1.23A^{1/3} - 0.60$ fm [22].

Now that we have all of the necessary parts of the scattering rate formula, the form of $\frac{dR}{dE_R}$ that will be most useful in Section 3 is:

$$\frac{dR}{dE_R} = \frac{\rho_\chi}{m_N m_\chi} \int_{v_{min}}^{v_{max}} \frac{\tilde{f}(\mathbf{v}, t)}{v} \frac{d\sigma}{dE_R} d^3 v \tag{17}$$

2.2 Electron Case

Current direct detection experiments are generally restricted to dark matter masses on the scale of GeV or higher, because in order to detect the nuclear recoils, the recoil energy must be above a certain threshold and sub-GeV dark matter particles generally do not produce collisions with high enough energies [25]. The DM-electron scattering paradigm, however, is promising for detecting sub-GeV dark matter particles, since DM-electron scattering is inelastic by nature. This implies that a larger fraction of the dark matter particle's energy is transferred to the electron in the collision and ionization signals can theoretically be detected. For DM-electron detection experiments, detection is restricted to masses on the scale of several MeV [26].

2.2.1 Dark Matter-Electron Kinematics

Consider a collision between a dark matter particle and a bound electron, where the transferred energy excites the electron to either a higher-energy bound state or an ionized state. A bound state electron, unlike the nucleus of the previous section, does not have definite momentum, and could in fact have arbitrarily high momentum, so the kinematics for this case are very different from those in the previous section. We can still find the energy transferred to the electron by the DM particle in terms of the momentum lost by the DM particle, $\vec{q}$ (see Fig. 3):

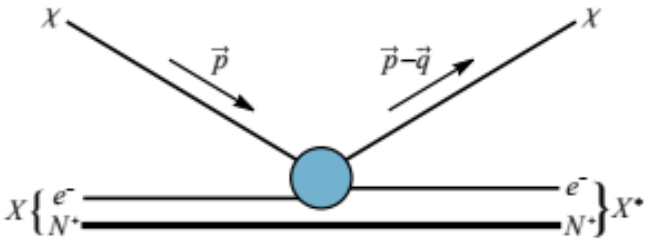

Figure 3: DM-electron scattering. Dark matter particle with momentum $\vec{p}$ excites a bound electron from ground state X to excited state X^*, transferring momentum $\vec{q}$ in the process. Figure from [26].

$$\Delta E_e = -\Delta E_\chi - \Delta E_N, \tag{18}$$

where the ΔE_χ is the change in energy in the DM particle and the ΔE_N is from the recoil of the entire atom. The energy transfer for the DM particle is given by:

$$\Delta E_\chi = \frac{|m_\chi \vec{v} - \vec{q}|^2}{2m_\chi} - \frac{1}{2} m_\chi v^2,$$

and by conservation of momentum, ΔE_N is:

$$\Delta E_N = \frac{q^2}{2m_N}.$$

The recoil of the atom is relatively small, so we can say $\Delta E_N = -\Delta E_\chi$ in practice and assume that the reduced mass $\mu_{\chi N} \sim m_N$:

$$\Delta E_e = -\Delta E_\chi = -\frac{|m_\chi \vec{v} - \vec{q}|^2}{2m_\chi} + \frac{1}{2} m_\chi v^2 - \frac{q^2}{2m_N} \tag{19}$$

$$= \vec{q} \cdot \vec{v} - \frac{q^2}{2\mu_{\chi N}} \tag{20}$$

$$\cong \vec{q} \cdot \vec{v} - \frac{q^2}{2m_\chi}. \tag{21}$$

ΔE_e can be bounded by maximizing this equation with respect to $\vec{q}$ to find the maximum allowed energy transfer, which corresponds to *all* the kinetic energy of the collision exciting the electron:

$$\Delta E_e \leq \frac{1}{2} \mu_{\chi N} v^2 \approx \frac{1}{2} m_\chi v^2, \tag{22}$$

Or,

$$m_\chi \geq \frac{2\Delta E_e}{v^2}. \tag{23}$$

As long as m_χ is above this bound, the $\vec{q} \cdot \vec{v}$ term in equation (20) dominates, so the minimum momentum transfer q_{min} required for an energy transfer of ΔE_e can be expressed as:

$$q_{min} \geq \frac{\Delta E_e}{v} \tag{24}$$

The energy transfer to the electron ΔE_e contributes to both the electron recoil energy E_{er} and to overcoming the binding energy of the electron in its initial bound state i, $-E_b^i$:

$$\Delta E_e = E_{er} + E_b^i$$

Returning to the conservation of energy equation (19), we can find an expression for the minimum dark matter velocity required for electron recoil E_{er} by taking the momentum transfer to be parallel to the initial dark matter velocity, and taking the $\frac{q^2}{2m_N}$ term to be small (since the recoil of the atom is relatively small):

$$E_{er} + E_b^i = -\frac{(m_\chi v_{min} - q)^2}{2m_\chi} + \frac{1}{2}\frac{(m_\chi v_{min})^2}{m_\chi},$$

Solving for v_{min} gives:

$$v_{min} = \frac{E_{er} + E_b^i}{q} + \frac{q}{2m_\chi}. \tag{25}$$

Note from this equation that the minimum DM velocity required to excite an electron with recoil energy E_{er} depends on the bound-state energy of the target electron.

2.2.2 Electron Scattering Rate Calculation

Just as the dark matter-nucleus collision is parameterized by the DM-nucleon scattering cross section, σ_p, in Section 2.1.2, the strength of the dark matter-electron interaction is parameterized by the DM-electron cross section, σ_e. If the interaction is totally independent of the momentum transfer q, then the DM-electron cross section is that of dark matter scattering with a free electron [26], but generally, the momentum transfer dependence needs to be accounted for in the rate calculation.

To account for the q dependence of this interaction, we must consider the dark matter form facter, $F_{DM}(q)$. The two most interesting limits of the form factor are found when considering the case of dark matter scattering through a dark photon mediator. When the dark-photon mass is large compared to the momentum transfer q, the DM form factor assumes the limit $F_{DM}(q) = 1$, and σ_e is the free elastic scattering DM-electron cross section. When the dark-photon is light or essentially massless compared to the momentum transfer, the form factor is $F_{DM}(q) = \alpha^2 m_e^2/q^2$ [27]. Following [25], the momentum-transfer dependence can be captured in defining the cross section in terms of the matrix element for DM-electron free elastic scattering for momentum transfer $q = \alpha m_e$, $\mathcal{M}_{free}(\alpha m_e)$, so that:

$$\overline{|\mathcal{M}_{\text{free}}(\vec{q})|^2} \equiv \overline{|\mathcal{M}_{\text{free}}(\alpha m_e)|^2} \times |F_{DM}(q)|^2$$

$$\sigma_e \equiv \frac{\mu_{\chi e}^2 |\mathcal{M}_{\text{free}}(\alpha m_e)|^2}{16\pi m_\chi^2 m_e^2},$$

where the absolute values of the matrix elements are squared and averaged over initial particle spins and summed over final particle spins, and $\mu_{\chi e}$ is the reduced DM-electron mass.

The non-differential excitation rate for a DM-electron interaction, for some given electron transition from energy level 1 to energy level 2, can be written analagously to the basic DM-nucleus rate, averaging over the DM velocity distribution:

$$R_{1\to 2} = \frac{\rho_\chi}{m_\chi} \int f(\boldsymbol{v})(\sigma v)_{1\to 2} d^3v, \tag{26}$$

where now we are treating the ionization cross section times the DM speed, $(\sigma v)_{1\to 2}$, as the effective cross-section for this interaction.

Unlike in the nuclear case, the differential scattering rate for DM-electron excitation necessitates that we sum over the differential cross sections for all possible initial electron states. The equation for the differential cross section is derived fully in Appendix A of [25] using field theory, but for the purposes of this paper and in the next section, I will use the formula presented in [28] (also in [27]) for $\frac{d\langle\sigma^i{}_{ion} v\rangle}{d\ln E_{er}}$, the differential version of the ionization cross section times DM speed averaged over the DM velocity distribution:

$$\frac{d\langle\sigma^i{}_{ion} v\rangle}{d\ln E_{er}} = \frac{\sigma_e}{8\mu_{e\chi}^2} \int q \left| f^i_{ion}(k', q)\right|^2 |F_{DM}(q)|^2 \eta(v_{min}, t) dq, \tag{27}$$

where $\left|f^i_{ion}(k', q)\right|^2$ is the ionization form factor, which depends on the initial state i and momentum of the final state, k', after some momentum transfer q, $F_{DM}(q)$ is the dark matter form factor as discussed above, and and $\eta(v_{min}, t)$ is the mean inverse speed function of the incoming dark matter.

The ionization form factor $\left|f^i_{ion}(k', q)\right|^2$ accounts for the probability that some given momentum transfer q will cause a particular electron recoil energy E_{er}. If the final state of the electron is a plane wave, then we have $k' = \sqrt{2m_e E_{er}}$, and the ionization form factor for an atomic target with spherically symmetric full shells with quantum numbers (n, ℓ) is given by [27]:

$$\left|f^{n,\ell}_{ion}(k', q)\right|^2 = \frac{(2\ell+1)k'^2}{4\pi^3 q} \int k |\chi_{n,\ell}(k)|^2 dk, \tag{28}$$

where $\chi_{n,\ell}(k)$ is the radial bound-state wave function in momentum space, and the integral runs over $k = |k' \pm q|$ (as in [27, 28]).

The differential cross section also includes an integral over the astrophysical mean inverse speed function, $\eta(v_{min}, t)$, which is commonly defined as:

$$\eta(v_{min}, t) \equiv \int_{v_{min}}^{\infty} \frac{\tilde{f}(\boldsymbol{v}, t)}{v} d^3v, \tag{29}$$

where $\tilde{f}(\boldsymbol{v}, t)$ is the lab-frame DM velocity distribution as defined in Section 2.1. Again, η has a time dependence because $\tilde{f}$ has a time dependence based on time of year, but we

can (and will) choose to take its value for June in the next section.

Now, we can write the differential scattering rate $\frac{dR}{d\ln E_{er}}$ in terms of a sum over all possible initial electron states:

$$\frac{dR}{d\ln E_{er}} = N_T \frac{\rho_\chi}{m_\chi} F(k') \sum_i \frac{d\langle \sigma^i{}_{ion} v \rangle}{d\ln E_{er}}, \tag{30}$$

where N_T is the number of target nuclei, ρ_χ is the local dark matter density, and $F(k')$ is the Fermi factor, which corrects for the distortion of the wave function of the scattered electron by the atom itself. The non-relativistic equation for this factor is:

$$F(k') = \frac{2\pi\nu}{1 - e^{2\pi\nu}}, \tag{31}$$

where $\nu = Z_{eff}(\alpha m_e/k')$, α is the fine-structure constant, and Z_{eff} is the effective charge felt by the electron. As a reasonable approximation, we can set $Z_{eff} = 1$ [27].

3 Scattering Rates Using The Empirical RAVE-TGAS Velocity Distribution

In [18], the empirical velocity distributions found from studying stars in the metal-poor halo are used to calculate the event rate for DM-nucleus scattering. For this section, I repeat this calculation for the nuclear case in order to plot the function $g(v_{min})$, which is proportional to the scattering rate. I then apply the empirical velocity distribution to the electron scattering case, assuming an atomic Xenon target.

3.1 Nuclear Case

For the DM-nucleus interaction, we can examine the rate equation (17) and the cross-section equation (15) to find that, since the differential scattering cross-section $\frac{d\sigma}{dE_R}$ is proportional to $\frac{1}{v^2}$, the differential scattering rate $\frac{dR}{dE_R}$ is thus proportional to the function $g(v_{min})$:

$$g(v_{min}) = \int_{v_{min}}^{\infty} \frac{\tilde{f}(v)}{v} dv,$$

and we can use this function to represent the scattering rate, independent of the nuclear target.

Fig. 4 shows the RAVE-TGAS distribution for the [Fe/H]< -1.8 iron abundance cut and the Standard Halo Model in the heliocentric frame, alongside the $g(v_{min})$ function plotted for these two velocity distributions. As shown in [13], the scattering rate for the empirical distribution is higher than that of the SHM by $\sim 10\%$ for velocities under ~ 200km/s, and lower than that of the SHM by $\sim 40 - 50\%$ for larger velocities. Since the minimum

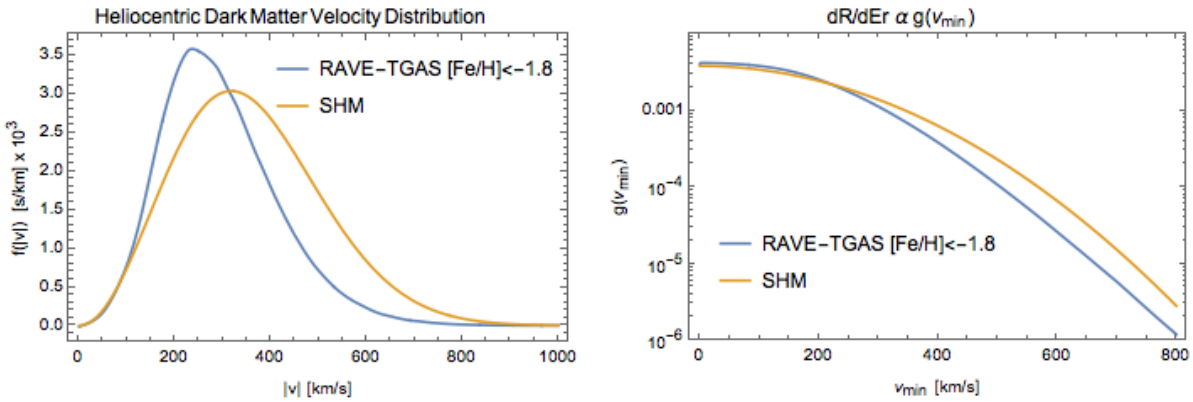

Figure 4: (*left*) Dark matter velocity distributions $f(|v|)$ in the heliocentric frame: [Fe/H] < -1.8 distribution (blue) and Standard Halo Model (yellow). (*right*) The function $g(v_{min})$ is plotted on a logarithmic scale with respect to minimum scattering velocity, using both velocity distributions.

DM speed for the nuclear scattering case is given by $v_{min} = \sqrt{\frac{m_N E_R}{2\mu^2}}$, for a given target nucleus, v_{min} is sensitive to the threshold energy E_R and the dark matter mass m_χ of the particular experiment.

For experiments with higher energy thresholds or lower DM masses, v_{min} is larger and thus $g(v_{min})$ integrates over (and is sensitive to) the high-speed tail of the DM velocity distribution $\tilde{f}(v)$. For example, the XENON1T experiment [29] uses a nuclear Xenon target and has a recoil energy threshold of $E_R = 5$ keV. At this energy threshold, for a DM mass of $m_\chi = 50$ GeV, the minimum DM speed would be $v_{min} \sim 150m/s$. We can see in Fig. 4 on the right that at this value of v_{min}, the scattering rate would be approximately the same for both the SHM and empirical velocity distributions. For a lower DM mass, however, such as $m_\chi = 10$ GeV, v_{min} is closer to 600 km/s and scattering rate using the empirical distribution gives a rate approximately two times smaller than that from the SHM [13].

3.2 Electron Case

In applying the empirical RAVE-TGAS [Fe/H]< -1.8 dark matter distribution to the DM-electron scattering case, several assumptions must be made. We assume that the target is an electron in the $5p$ shell of a Xenon atom. The ionization form factor then requires that we know the radial momentum-space bound-state wave functions for the $5p$ states in Xenon. For this calculation, following [27], the Roothaan-Hartree-Fock (RHF) ground-state wave functions are used. The RHF wave functions, in position-space, take the form:

$$R_{n,\ell}(r) = \sum_j C_{j\ell n} r^{n_{j\ell}-1} e^{\zeta_{j\ell} r}$$

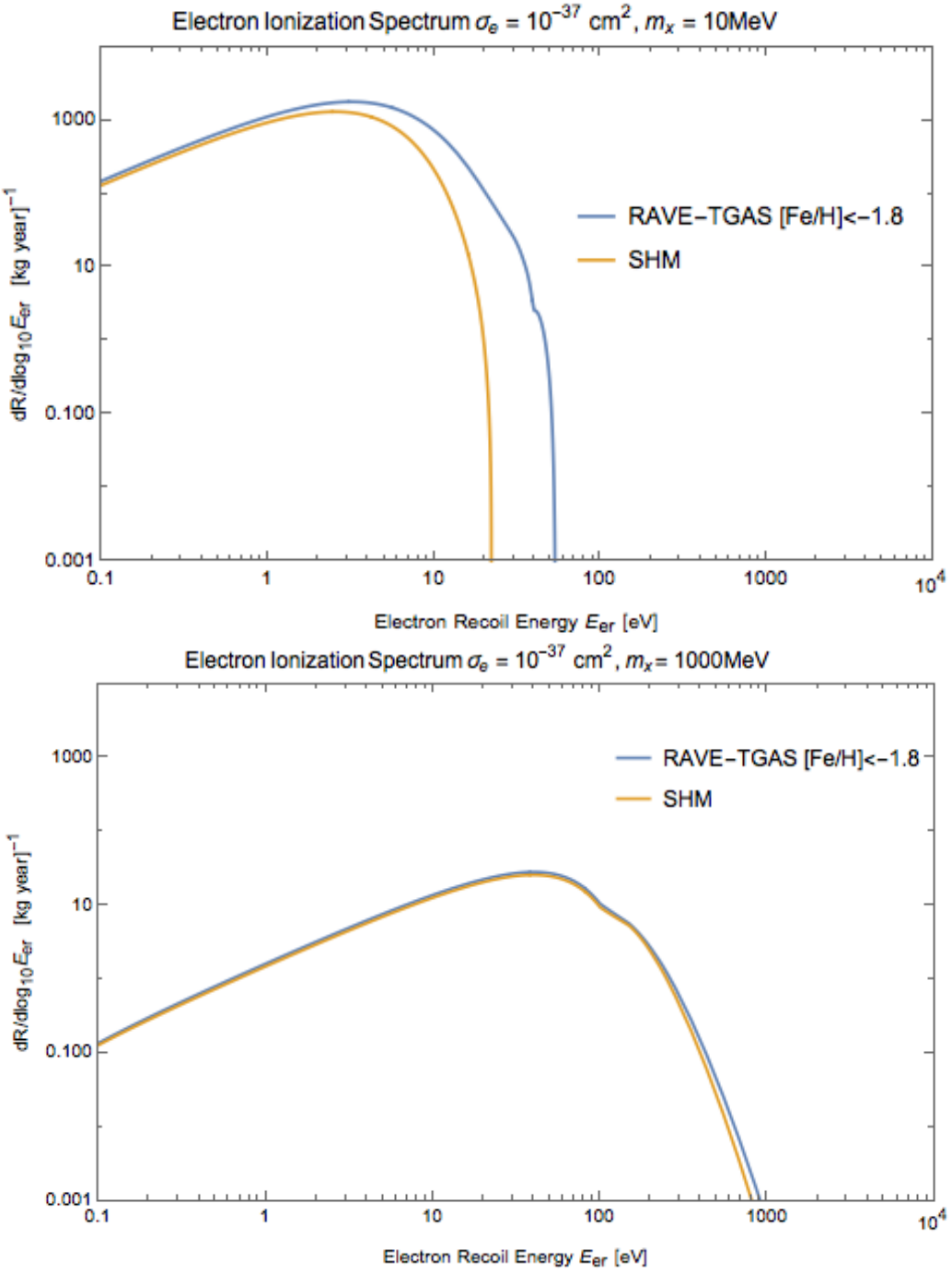

Figure 5: Differential event rates for a DM-electron scattering with a Xenon target, assuming a DM form factor $F_{DM}(q) = 1$ and a cross section $\sigma_e = 10^{-37}$ cm^2. Only the $5p$ orbital was used to calculate these rates. The rates are shown for DM masses of 10 MeV (top) and 1000 MeV (bottom). The blue lines represent the rates calculated using the empirical RAVE-TGAS [Fe/H] < -1.8 DM velocity distribution given in [18], and the yellow lines represent the rates calculated using the SHM.

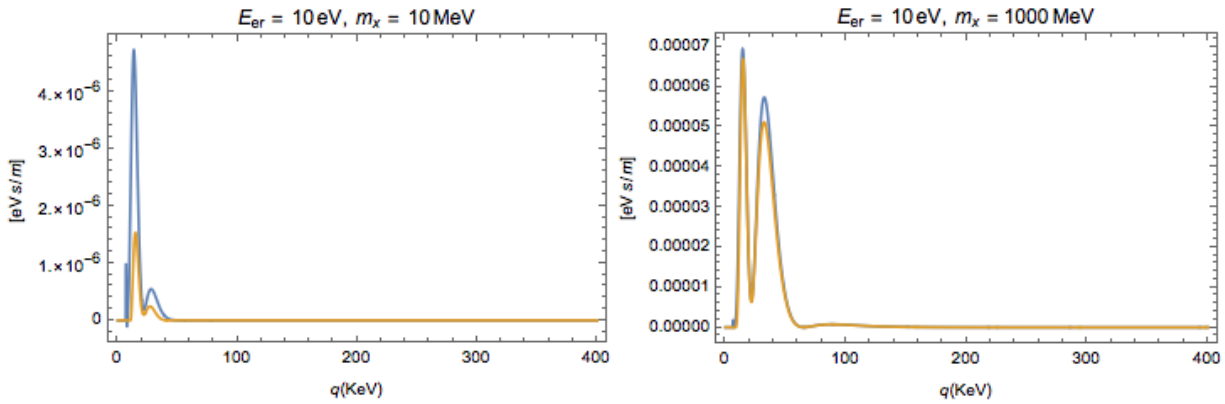

Figure 6: The integrand of the scattering rate equation, as a function of q and plotted for $E_{er} = 10$ eV and for $m_\chi = 10$ MeV (*left*) and 1000 MeV (*right*), approaches the same function for both the SHM (yellow) and empirical (blue) velocity distributions as DM mass increases.

where the coefficients $C_{j\ell n}$ can be found for the Xenon $5p$ states in [30]. Analytic expressions for $R_{n,\ell}(r)$ and $\chi_{n,\ell}(k)$ can also be found in Appendix C of [31]. Equipped with the analytic form of $\chi_{5,1}(k)$, the ionization form factor for this case simplifies to:

$$\left|f_{ion}^{5,1}(k',q)\right|^2 = \frac{3k'^2}{4\pi^3 q}\int_{|k'-q|}^{|k'+q|} k|\chi_{5,1}(k)|^2 dk,$$

where $k' = \sqrt{2m_e E_{er}}$. For the mean inverse speed function, we can directly use the form of $\eta(v_{min}, t)$ from Section 2.2.2, and eliminating the time dependence by assuming values of η for June 2nd. Also, for the purposes of this calculation, the graphs were produced using the limit of the DM form factor $F_{DM}(q) = 1$, and for the DM-electron cross section σ_e, a value of 10^{-37} cm^2 is used [27]. As mentioned above, for the Fermi factor we set $Z_{eff} = 1$, and the value of the fine-structure constant $\alpha \sim 1/137$ can be found in [32]. These are all of the necessary constants and parameters required to calculate the scattering rate for a given dark matter mass m_χ and electron recoil energy E_{er}.

Fig. 5 shows the differential scattering rate, plotted against the electron recoil energy E_{er}, for dark matter masses $m_\chi = 10$ MeV (top panel) and $m_\chi = 1000$ MeV (bottom panel) and a Xenon atomic target. Note that, at higher electron recoil energies, the empirical velocity distribution produces increasingly higher scattering rates than the SHM, and the difference between the two rates is much more pronounced for lower DM masses.

Recall the equation for v_{min} derived above:

$$v_{min} = \frac{E_{er} + E_b^i}{q} + \frac{q}{2m_\chi}.$$

At lower DM masses, v_{min} increases (as in the nuclear case), and so the integral in $\eta(v_{min})$ becomes more sensitive to the high-speed tail of the velocity distribution $\tilde{f}(v)$. For a given

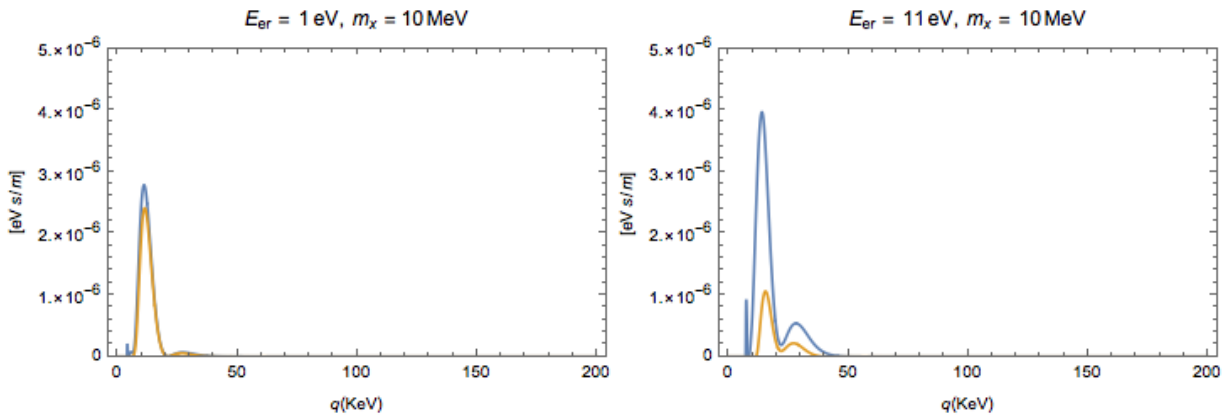

Figure 7: The integrand is plotted for $m_\chi = 10$ MeV and for $E_{er} = 1$ eV (*left*) and 11 eV (*right*). The integrand for the empircal velocity distribution (blue) becomes relatively much larger than that for the SHM (yellow) at higher electron recoil energies.

recoil energy E_{er}, the values of η for the SHM and empirical distributions approach each other as DM mass increases. Thus, the integrands of the rate equation for the SHM and empirical distributions (for $F_{DM} = 1$),

$$q\left|f_{ion}^{5p}(\sqrt{2m_e E_{er}}, q)\right|^2 \eta(v_{min}, t) \tag{32}$$

become increasingly close as DM mass increases. This is shown in Fig. 6, for $E_{er} = 10$ MeV. Similarly, exciting higher-energy transitions with larger values of E_{er} (for a given DM mass) also requires probing the tail of the DM velocity distribution. As a result, as E_{er} increases, η for the empirical distribution becomes larger relative to η for the SHM distribution, and the integrand (32) does the same. This is shown in Fig. 7.

4 Conclusion

Light dark matter (in the MeV to GeV range) is becoming an increasingly important candidate to explore in the realm of direct detection experiments. While sub-GeV dark matter is too light to create detectable nuclear recoils, the DM-electron scattering paradigm allows for much lighter DM masses to create detectable ionization signals. I reviewed the physics behind both DM-nucleus scattering direct detection experiments and DM scattering off an electron in an atomic target. In particular, I compared the scattering rates for these interactions calculated using both the commonly-used Standard Halo Model DM velocity distribution and the empirical RAVE-TGAS [Fe/H]< -1.8 distribution produced in [18] by using metal-poor stars as a tracer and studying their kinematics.

For the electron case, I found that the empirical distribution produces higher scattering rates than the Standard Halo Model at higher recoil energies, and that this difference also becomes more pronounced for lower DM masses. The discrepancy at high recoil energies is particularly relevant to direct detection experiments because these experiments

have energy thresholds below which they cannot detect scattering events (for example, the XENON1T experiment has an energy threshold of $E_R = 5$ keV) [29]. Even more promising is the case of dark matter scattering off of electrons in a semiconductor target, in which the energy threshold required for electron ionization is reduced by up to a factor of 20 [25]. The DM-electron scattering rate for a semiconductor target using the empirical velocity distribution was not examined for this paper, but this is the natural next step and would be a worthwhile calculation.

References

[1] P. A. R. Ade et al. Planck 2015 results. XIII. Cosmological parameters. *Astron. Astrophys.*, 594:A13, 2016.

[2] V. C. Rubin, N. Thonnard, and W. K. Ford, Jr. Rotational properties of 21 SC galaxies with a large range of luminosities and radii, from NGC 4605 /R = 4kpc/ to UGC 2885 /R = 122 kpc/. *Astrophys. J.*, 238:471, 1980.

[3] Mariangela Lisanti. Lectures on Dark Matter Physics. In *Proceedings, Theoretical Advanced Study Institute in Elementary Particle Physics: New Frontiers in Fields and Strings (TASI 2015): Boulder, CO, USA, June 1-26, 2015*, pages 399–446, 2017.

[4] J. Binney and S. Tremaine. *Galactic Dynamics*. Princeton University Press, 2008.

[5] Martin C. Smith et al. The RAVE Survey: Constraining the Local Galactic Escape Speed. *Mon. Not. Roy. Astron. Soc.*, 379:755–772, 2007.

[6] Andrew R. Wetzel, Philip F. Hopkins, Ji-hoon Kim, Claude-Andre Faucher-Giguere, Dusan Keres, and Eliot Quataert. Reconciling dwarf galaxies with ΛCDM cosmology: Simulating a realistic population of satellites around a Milky Way-mass galaxy. *Astrophys. J.*, 827(2):L23, 2016.

[7] J. Diemand, M. Kuhlen, P. Madau, M. Zemp, B. Moore, D. Potter, and J. Stadel. Clumps and streams in the local dark matter distribution. *Nature*, 454:735–738, 2008.

[8] Joachim Stadel, Doug Potter, Ben Moore, Jurg Diemand, Piero Madau, Marcel Zemp, Michael Kuhlen, and Vicent Quilis. Quantifying the heart of darkness with GHALO - a multi-billion particle simulation of our galactic halo. *Mon. Not. Roy. Astron. Soc.*, 398:L21–L25, 2009.

[9] Volker Springel, Jie Wang, Mark Vogelsberger, Aaron Ludlow, Adrian Jenkins, Amina Helmi, Julio F. Navarro, Carlos S. Frenk, and Simon D. M. White. The Aquarius Project: the subhalos of galactic halos. *Mon. Not. Roy. Astron. Soc.*, 391:1685–1711, 2008.

[10] Michael Kuhlen, Neal Weiner, Jurg Diemand, Piero Madau, Ben Moore, Doug Potter, Joachim Stadel, and Marcel Zemp. Dark Matter Direct Detection with Non-Maxwellian Velocity Structure. *JCAP*, 1002:030, 2010.

[11] Javiera Guedes, Simone Callegari, Piero Madau, and Lucio Mayer. Forming Realistic Late-Type Spirals in a LCDM Universe: The Eris Simulation. *Astrophys. J.*, 742:76, 2011.

[12] Mark Vogelsberger, A. Helmi, Volker Springel, Simon D. M. White, Jie Wang, Carlos S. Frenk, Adrian Jenkins, A. D. Ludlow, and Julio F. Navarro. Phase-space structure in the local dark matter distribution and its signature in direct detection experiments. *Mon. Not. Roy. Astron. Soc.*, 395:797–811, 2009.

[13] Jonah Herzog-Arbeitman, Mariangela Lisanti, Piero Madau, and Lina Necib. Empirical Determination of Dark Matter Velocities using Metal-Poor Stars. 2017.

[14] Julio F. Navarro, Carlos S. Frenk, and Simon D. M. White. The Structure of cold dark matter halos. *Astrophys. J.*, 462:563–575, 1996.

[15] J. Einasto. *Trudy Astrofizicheskogo Instituta Alma-Ata*, 5:87–100, 1965.

[16] Alister W. Graham, David Merritt, Ben Moore, Juerg Diemand, and Balsa Terzic. Empirical models for Dark Matter Halos. I. Nonparametric Construction of Density Profiles and Comparison with Parametric Models. *Astron. J.*, 132:2685–2700, 2006.

[17] Zeljko Ivezic et al. The Milky Way Tomography with SDSS. 2. Stellar Metallicity. *Astrophys. J.*, 684:287–325, 2008.

[18] Jonah Herzog-Arbeitman, Mariangela Lisanti, and Lina Necib. The Metal-Poor Stellar Halo in RAVE-TGAS and its Implications for the Velocity Distribution of Dark Matter. 2017.

[19] Gaia Collaboration. The Gaia Mission. *Astronomy and Astrophysics*, 595, 2016.

[20] A. Kunder et al. The Radial Velocity Experiment (RAVE): Fifth Data Release. *Astronomical Journal*, 2016.

[21] Katherine Freese and Christopher Savage. Dark Matter collisions with the Human Body. *Phys. Lett.*, B717:25–28, 2012.

[22] J. D. Lewin and P. F. Smith. Review of mathematics, numerical factors, and corrections for dark matter experiments based on elastic nuclear recoil. *Astropart. Phys.*, 6:87–112, 1996.

[23] Samuel K. Lee, Mariangela Lisanti, and Benjamin R. Safdi. Dark-Matter Harmonics Beyond Annual Modulation. *JCAP*, 1311:033, 2013.

[24] Richard H. Helm. Inelastic and Elastic Scattering of 187-Mev Electrons from Selected Even-Even Nuclei. *Phys. Rev.*, 104:1466–1475, 1956.

[25] Rouven Essig, Marivi Fernandez-Serra, Jeremy Mardon, Adrian Soto, Tomer Volansky, and Tien-Tien Yu. Direct Detection of sub-GeV Dark Matter with Semiconductor Targets. *JHEP*, 05:046, 2016.

[26] Rouven Essig, Aaron Manalaysay, Jeremy Mardon, Peter Sorensen, and Tomer Volansky. First Direct Detection Limits on sub-GeV Dark Matter from XENON10. *Phys. Rev. Lett.*, 109:021301, 2012.

[27] Samuel K. Lee, Mariangela Lisanti, Siddharth Mishra-Sharma, and Benjamin R. Safdi. Modulation Effects in Dark Matter-Electron Scattering Experiments. *Phys. Rev.*, D92(8):083517, 2015.

[28] Rouven Essig, Jeremy Mardon, and Tomer Volansky. Direct Detection of Sub-GeV Dark Matter. *Phys. Rev.*, D85:076007, 2012.

[29] E. Aprile et al. First Dark Matter Search Results from the XENON1T Experiment. *Phys. Rev. Lett.*, 119(18):181301, 2017.

[30] C. F. Bunge, J. A. Barrientos, and A. V. Bunge. Roothaan-Hartree-Fock Ground-State Atomic Wave Functions: Slater-Type Orbital Expansions and Expectation Values for Z = 2-54. *Atom. Data Nucl. Data Tabl.*, 53:113–162, 1993.

[31] Joachim Kopp, Viviana Niro, Thomas Schwetz, and Jure Zupan. DAMA/LIBRA and leptonically interacting Dark Matter. *Phys. Rev.*, D80:083502, 2009.

[32] C. Patrignani et al. Review of Particle Physics. *Chin. Phys.*, C40(10):100001, 2016.